Journal of Materials Chemistry A

COMMUNICATION

View Article Online
View Journal | View Issue

Cite this: J. Mater. Chem. A, 2015, 3, 15408

Received 30th April 2015
Accepted 1st July 2015

DOI: 10.1039/c5ta03184b

www.rsc.org/MaterialsA

Elastic ionogels with freeze-aligned pores exhibit enhanced electrochemical performances as anisotropic electrolytes of all-solid-state supercapacitors†

Xinhua Liu,[a] Baofeng Wang,*[b] Zilu Jin,[a] Huanlei Wang[c] and Qigang Wang*[a]

Bio-inspired by bone materials, hierarchical porous materials with aligned structure have been designed and applied in various fields. However, the realization of anisotropic function based on aligned structures is still a challenge. Herein, we prepare nanocomposite ionogel electrolytes with aligned porous structures *via* a directional freezing of $BMIMPF_6$, PEGMA (PEGDA), and TiO_2 at −18 °C and further TiO_2-initiated cryopolymerization under UV irradiation. The crystals of PEG derivatives at −18 °C provide a directional template for the formation of aligned porous structures within the ionogel networks. The additional TiO_2 nanoparticles, as photoinitiators and nanofillers, endow the aligned ionogels with high mechanical strength. The aligned ionogel-based supercapacitor exhibits anisotropic electrochemical performance and flexibility. The specific capacitance of the device with the vertically aligned ionogel is 172 F g^{-1} at the current density of 1 A g^{-1}, which is larger than those of the parallel aligned and non-aligned devices.

Bio-inspired by naturally aligned bone materials, aligned micrometre-sized porous materials have shown significant importance in biomedical engineering,[1] electronics,[2–4] and energy storage devices.[5–10] Ionic conducting polymer gels with aligned structures have promising applications in modern electronics and multidisciplinary fields due to their accelerated ionic transport in large pores, semi-solid state and flexibility compared to some inorganic solid electrolytes.[11–15] Conventional polymer electrolytes prepared by physical mixing and *in situ* polymerization methods can be used in flexible and portable electric devices, such as electro-active actuators,[16–18] supercapacitors,[19–22] lithium batteries,[23] dye sensitized solar cells[24] and fuel cells.[25] However, they can hardly balance the conflict between maintaining necessary mechanical strength and electrochemical properties due to the lack of hierarchical structure within the gel matrix. An aligned porous structure within ionogels can endow them with similar ionic conductivity to the pure ionic liquid in the vertical direction, combined with obvious enhanced thermal stability and mechanical strength.[26]

The ice-templating process is a simple yet versatile method to facilitate the preparation of extensive hierarchical porous materials.[27,28] Generally, a solution (or colloidal suspension) is frozen in cold liquid and then the porous structures are produced after freeze-drying to remove the solvent.[29,30] Cooper's group introduced a directional freezing approach employing building blocks (polymers, nanoparticles or their mixtures) to prepare aligned porous materials. This approach was claimed to be able to achieve both good mechanical properties and desired hierarchically porous structures perfectly.[31] As a pioneering example, Tomsia's group employed an ice-templating method and low-temperature polymerization to prepare thermo-responsive composite hydrogels with hierarchical structures.[32] Up to now, this approach has rarely been applied in the preparation of ionogels with high mechanical strength.

Herein, we designed simple directional templating ionogels with aligned porous structures. The aligned ionogels are appropriate electrolytes in flexible supercapacitors because of their excellent electrochemical behaviour from the aligned structures. The aligned ionogel electrolytes have the following components: 1-*N*-butyl-3-methylimidazolium hexafluorophosphate ($BMIMPF_6$), TiO_2 nanoparticles (TiO_2-NPs), and poly(ethylene glycol) methacrylate (PEGMA, M_n = 500) consisting of 5 wt% poly(ethylene glycol) dimethacrylate (PEGDA, M_n = 700) (shown in Fig. 1a). PEGMA and PEGDA were chosen as the crystal temple considering their high melting points at about 25 °C.[33] Ionic liquids $BMIMPF_6$, 1-butyl-3-methylimidazolium bis[(trifluoromethyl)sulfonyl]imide (BMIMTFSI), and 1-butyl-3-methyl imidazolium tetrafluoroborate ($BMIMBF_4$) were selected because of their different

[a]Department of Chemistry and Advanced Research Institute, Tongji University, Shanghai 200092, P. R. China. E-mail: wangqg66@tongji.edu.cn

[b]College of Environmental and Chemical Engineering, Shanghai University of Electric Power, Shanghai 200090, P. R. China. E-mail: wangbaofeng@shiep.edu.cn

[c]Institute of Materials Science and Engineering, Ocean University of China, Qingdao 266100, P. R. China

† Electronic supplementary information (ESI) available: The detailed experimental procedures, sample pre-treatments and various characterizations are provided. See DOI: 10.1039/c5ta03184b

melting points and excellent electrochemical properties. TiO_2 nanoparticles were used as the photoinitiator for the polymerization of monomers and as a reinforced nanofiller to enhance the mechanical strength of the ionogel *via* the supramolecular effect.[34–36]

As an example, 0.005 g TiO_2-NPs and 0.100 g PEGMA (PEGDA) were dissolved in 0.895 g $BMIMPF_6$ *via* magnetic stirring for 30 min to form a viscous solution (Fig. 1c). Holes (h^+) and electrons can be generated from the TiO_2-NPs under UV irradiation (Fig. 1b) after which the electrons can be entrapped either by $BMIM^+$ or the cavity in the ionic liquid to form solvated electrons, and the holes can serve as initiators to react with the monomers.[18,36] Furthermore, the radicals of the chain growth can be validated by electron paramagnetic resonance (EPR) spectroscopy through UV irradiation (Fig. S1, ESI†). The gelation kinetics were further confirmed by using time sweep measurements for monitoring the crossover points between the storage modulus (G') and the loss modulus (G'') (Fig. S2, ESI†). The frequency sweep curves illustrate substantial gel-like elastic responses ($G' > G''$) of the ionogels with various TiO_2 contents (Fig. S3, ESI†). In this case, the final conversion of the monomers was over 93% after 2.5 hours of UV irradiation (Fig. S4, ESI†).

Finally, an aligned ionogel can be obtained through UV cryopolymerization of the solid precursor for 2.5 hours at a temperature of −18 °C (Fig. 1e). The cold UV light (with an average intensity of 99.8 mW cm^{-2} at 365 nm) was selected in the cryopolymerization process to avoid any possible thermal impacts. Fig. S5, ESI† shows the changes of G' and G'' of the aligned ionogels as a function of the angular frequency, which also indicate a gel-like elastic performance.

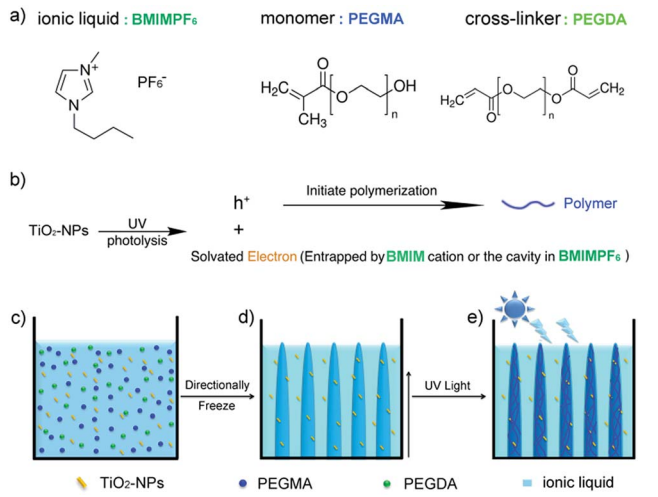

Fig. 1 Proposed mechanism of the crosslinked aligned ionogel from a monomer precursor solution. (a) The molecular structures. (b) The mechanism of the TiO_2-NPs initiated UV polymerization. (c) The precursor solution. (d) The ionic liquid molecules are excluded during directional freezing between the orientated monomer crystals. (e) The monomers are polymerized in the frozen state to produce an aligned structure.

The scanning electron microscope (SEM) images in Fig. 2a–c demonstrate the porous structures of the ionogels. Vertically aligned structures were observed in the cryopolymerized ionogels which were frozen directionally. As a control experiment, polymerized samples without directional freezing cannot form an aligned structure. The PEG-based monomers can be directionally frozen in a reactor maintained at a temperature of about −18 °C (in Fig. S6, ESI†). The aligned structures in Fig. 2b and c can be attributed to the directional crystals of monomers.

As shown in Fig. 2d and S7,† the ionogels display good mechanical strength in compressive tests and elastic response in loading–unloading curves. Compared to conventional initiators, the TiO_2-NPs with an average size of 25 nm (Fig. S8†) can also act as the inorganic cross-linking points for cryopolymerization of ionogels without any leakage of the ionic liquid (Fig. S9†).[34–36] When the amount of TiO_2-NPs was increased from 0.25 wt% to 0.5 wt%, the Young's modulus increased from 1.6 kPa to 21.2 kPa. The ionic conductivities of the ionogels with different TiO_2 contents have no great difference. The optimum amount of TiO_2-NPs is 0.5 wt%. The ionogel with specific aligned porous structures (aligned) is able to keep a similar high mechanical strength (Fig. S10, ESI†) relative to the non-aligned porous ionogel (non-aligned). These elastic ionogels are both designed as electrolytes for all solid-state supercapacitors.

Herein, carbon nanocages (CNC700) with a specific surface area of 1810 m^2 g^{-1} were selected as supercapacitor electrode materials.[37] The SEM, TEM, nitrogen sorption isotherms, and the pore size distributions are shown in Fig. S11 and S12 (ESI†). Two carbon nanocage electrodes and an ionogel film were sandwiched in an all-solid-state supercapacitor. The calculated ionic conductivity of the non-aligned ionogel was 1.06 mS cm^{-1} (Fig. S13, ESI†). In contrast, the ionogel with aligned structures provided a value of 1.46 mS cm^{-1}, which is close to that of pure $BMIMPF_6$ (1.57 mS cm^{-1}).[38] The aligned ionogel-based supercapacitor exhibits a more rectangular cyclic voltammogram curve than the non-aligned one (Fig. S14, ESI†), which implies

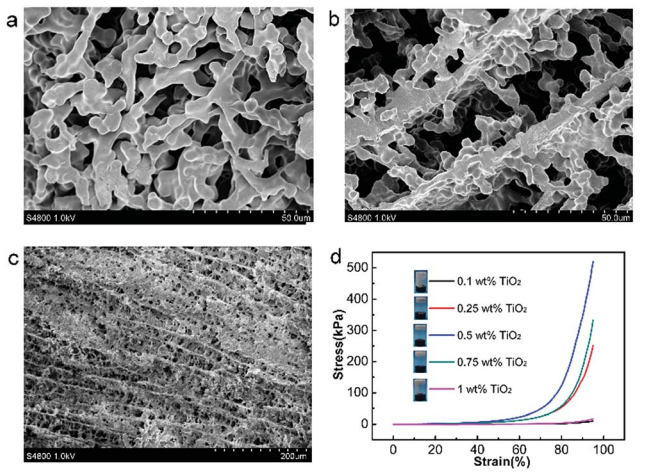

Fig. 2 SEM images of the three-dimensional composites after vacuum freeze-drying. (a) Non-aligned porous structure; (b and c) aligned porous structures; (d) compressive curves of the ionogels with different TiO_2 contents *via* cryopolymerization.

the enhanced electrochemical performance of the aligned device.

The charge and discharge curves are shown in Fig. 3a, which can be seen as the indication of capacitive performances. The aligned ionogel based supercapacitor achieved a high specific capacitances (C_{sp}) value of 172 F g^{-1} at the current density of 1 A g^{-1}, while the value of the non-aligned device was only 140 F g^{-1}. The aligned supercapacitor possesses fast charging and discharging behavior (Fig. S15, ESI†). It is obvious that the aligned ionogel-based device performed better in maintaining higher C_{sp} values at higher current densities than the non-aligned one (Fig. 3b). Notably, the electrochemical performance of the ionogel with regularly aligned structures is comparable to that of the pure ionic liquid electrolyte-based device, thus further advocating the use of the aligned structures in electrochemical applications. Fig. S16 and S17 (ESI†) also indicate the enhanced performance for aligned ionogel devices with BMIMTFSI and $BMIMBF_4$.

The enhanced electrochemical properties of the aligned ionogel can be attributed to easier ion transferring between electrode/electrolyte interfaces and quicker ionic mobility within the gel electrolyte. The different pore distributions of the aligned and non-aligned ionogels measured by the Hg intrusion (Fig. 4) may be the reason for the enhanced performance. The network of the aligned ionogel exhibits a 68.7% porosity, by utilizing ethanol to go into the pores, and regular pores at 1–2 and 8–10 micrometers, by mercury intrusion measurement. As the control, the network of a non-aligned ionogel has only 42.4% porosity and a wide pore distribution from 0.01–10 micrometers. The aligned ionogel with more effective large pores can host more free ions, thus they can accelerate ion transfer across the electrode/electrolyte interface and ion mobility within the electrolyte. However, the lower porosity and the existence of capillary pores within the non-aligned ionogel have a detrimental effect on ion movement across the interfaces and within the gel matrix.

As shown in Fig. 3c, the impedance spectra have an arc at the higher frequency area and a spike at the lower frequency area. The impedance plots of supercapacitors with different ionogel structures suggest the lower bulk resistance of the vertically aligned ionogel based supercapacitor. The bulk resistances mainly attributed to the ionogel electrolytes are found to be $R_{\text{b-aligned-2}} < R_{\text{b-aligned-1}} \approx R_{\text{b-non-aligned}}$. The different semicircles in the high frequency range correspond to the charge transfer resistance (R_{ct}) caused by the double layer capacitance on the surface. The Warburg resistance (Z_w) is the result of the frequency dependent ion transport. C_L is the limit capacitance. The results indicate that only the vertical direction can benefit the ion transport within the ionogel matrix and on the surface of the electrode materials. The resistances of the ionogels increase proportionally with the increased thickness, while the resistivities have no relation with the thicknesses of the ionogels (Fig. S13, ESI†).

The resistivity is anisotropic in the aligned ionogel. The vertical direction (aligned-2) and parallel directions (aligned-1) have 6.9 Ω m and 9.1 Ω m resistivity, respectively. The aligned-1 ionogel has similar resistivity to the non-aligned one (9.3 Ω m) due to the parallel pores, which could not provide effective ion pathways. The differences in ion pathways and resulting ionic mobility within various types of ionogels are described in eqn

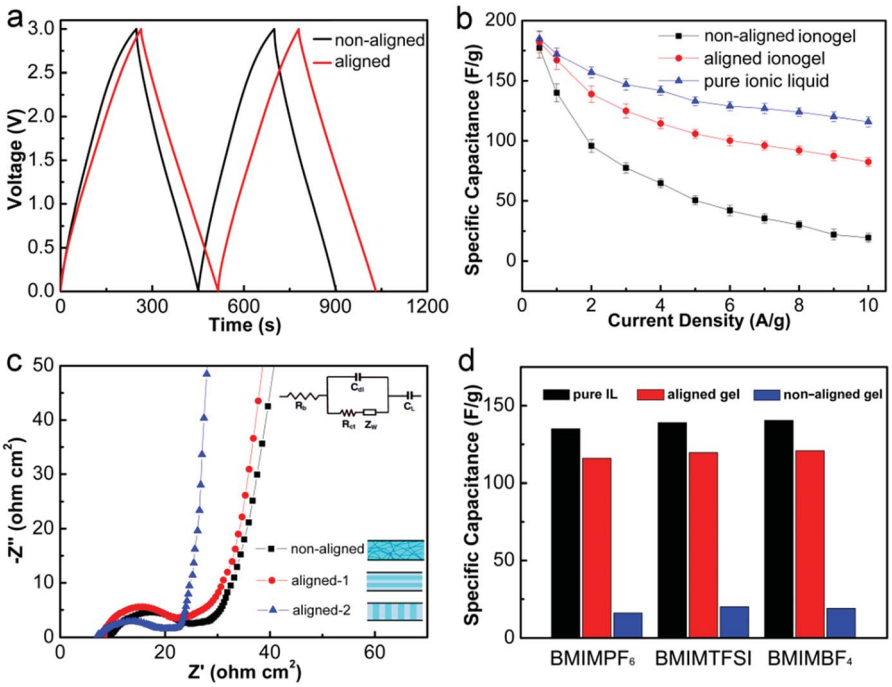

Fig. 3 Electrochemical properties. (a) Galvanostatic charge–discharge curves of the ionogel electrolyte based supercapacitors measured at 1 A g^{-1}. (b) The correlation of specific capacitance with various current densities. (c) The impedance plots of supercapacitors with different ionogel structures at room temperature. (d) The specific capacitances of supercapacitors with different electrolytes at −18 °C.

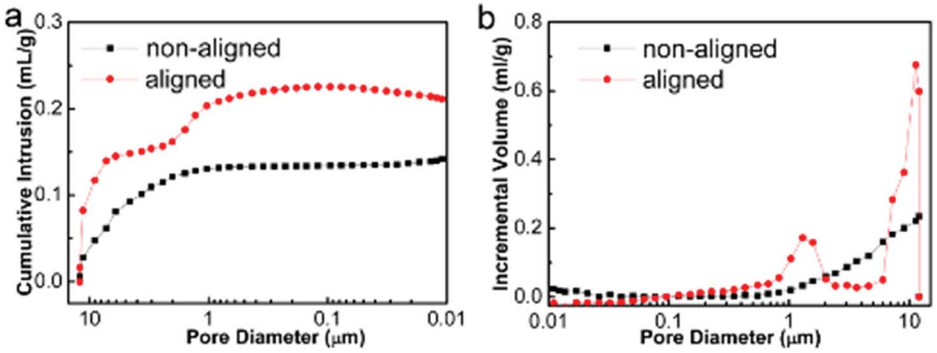

Fig. 4 Pore distribution of the aligned and non-aligned ionogels. (a) Hg cumulative intrusion, and (b) Hg incremental volume *versus* pore diameter of the aligned and non-aligned samples.

(S1) and Fig. S18, ESI.† To validate this assumption, the electrochemical properties of the ionogel with parallel aligned structures were measured. The parallel ionogel exhibits a similar ionic conductivity (1.02 mS cm^{-1}) and an equivalent specific capacitance (139 F g^{-1} at the current density of 1 A g^{-1}) to the non-aligned ionogel for the fabrication of supercapacitors. The results further illustrate the electrochemical enhancements of the vertically aligned ionogel based devices.

The aligned ionogel based supercapacitor possesses excellent capacitive performance over a wide temperature range from −18 °C to 200 °C (Fig. S19, ESI†). The pure ionic liquids, aligned ionogels, and non-aligned ionogels of these ionic liquids were used as electrolytes for supercapacitors at low temperature (−18 °C). Fig. 3d shows that the aligned ionogel supercapacitors can maintain high C_{sp} retention rates of 85%, 86% and 85% of the devices with corresponding pure ionic liquids at 0.05 A g^{-1}. However, the non-aligned devices had the lowest specific capacitance values. This easy ion transport near the porous electrode proves our previous hypothesis that the monomers are the real crystal temple for the alignment process. As shown in Fig. S20,† the ionic liquids fail to crystallize during the cooling process.[39] In order to further verify this assumption, the precursor was then frozen in liquid nitrogen *via* the same cryopolymerization. The obtained aligned ionogel based device also exhibited similar electrochemical performances (Fig. S21, ESI†). Further, the aligned ionogel based device demonstrated a good stability (Fig. S22, ESI†). Additionally, our flexible supercapacitors exhibited excellent mechanical and electrochemical robustness in various bending tests (Fig. S23, ESI†), indicating the potential of the flexible supercapacitors in practical applications.

In conclusion, ionogels with aligned porous structures are prepared by a directional freezing method and further cryopolymerization, and they possess significant improvement in electrochemical properties comparing to non-aligned ionogels. It is expected that the proposed method will be useful for the preparation of aligned ionic conducting ionogels combining the advantages of mechanical strength and electrochemical functions. The elastic ionogels with aligned pores have great potential to be integrated electrolytes and separators for the facile fabrication of various flexible energy devices.

Acknowledgements

This work was supported by the National Science Foundation of China (No. 21274111), the Program for New Century Excellent Talents in University of Ministry of Education of China (NECT-11-0386), the Fundamental Research Funds for Central Universities, and the Recruitment Program of Global Experts.

Notes and references

1 E. Salnikov, M. Rosay, S. Pawsey, O. Ouari, P. Tordo and B. Bechinger, *J. Am. Chem. Soc.*, 2010, **132**, 5940.
2 A. Yamaguchi, F. Uejo, T. Yoda, T. Uchida, Y. Tanamura, T. Yamashita and N. Teramae, *Nat. Mater.*, 2004, **3**, 337.
3 A. Walcarius, E. Sibottier, M. Etienne and J. Ghanbaja, *Nat. Mater.*, 2007, **6**, 602.
4 H. Gu, R. Zheng, X. Zhang and B. Xu, *Adv. Mater.*, 2004, **16**, 1356.
5 T. Chen, L. Qiu, H. G. Kia, Z. Yang and H. Peng, *Adv. Mater.*, 2012, **24**, 4623.
6 T. Chen, Z. Cai, L. Qiu, H. Li, J. Ren, H. Lin, Z. Yang, X. Sun and H. Peng, *J. Mater. Chem. A*, 2013, **1**, 2211.
7 T. Chen, L. Qiu, Z. Cai, F. Gong, Z. Yang, Z. Wang and H. Peng, *Nano Lett.*, 2012, **12**, 2568.
8 H. Wang, D. Kong, P. Johanes, J. J. Cha, G. Zheng, K. Yan, N. Liu and Y. Cui, *Nano Lett.*, 2013, **13**, 3426.
9 W. Weng, H. Lin, X. Chen, J. Ren, Z. Zhang, L. Qiu, G. Guan and H. Peng, *J. Mater. Chem. A*, 2014, **2**, 9306.
10 H. Lin, W. Weng, J. Ren, L. Qiu, Z. Zhang, P. Chen, X. Chen, J. Deng, Y. Wang and H. Peng, *Adv. Mater.*, 2014, **26**, 1217.
11 M. L. Hammock, A. Chortos, B. C. K. Tee, J. B. H. Tok and Z. Bao, *Adv. Mater.*, 2013, **25**, 5997.
12 Z. Yang, J. Deng, X. Chen, J. Ren and H. Peng, *Angew. Chem., Int. Ed.*, 2013, **52**, 13453.
13 P. Docampo, J. M. Ball, M. Darwich, G. E. Eperon and H. J. Snaith, *Nat. Commun.*, 2013, **4**, 2761, DOI: 10.1038/ncomms3761.
14 T. Tamura and H. Kawakami, *Nano Lett.*, 2010, **10**, 1324.
15 H. Xia, H. L. Wang, W. Xiao, M. O. Lai and L. Lu, *Int. J. Surf. Sci. Eng.*, 2009, **3**, 23.

16 K. Mukai, K. Asaka, K. Kiyohara, T. Sugino, I. Takeuchi, T. Fukushima and T. Aida, *Electrochim. Acta*, 2008, **53**, 5555.
17 B. He, Z. Wang, M. Li, K. Wang, R. Shen and S. Hu, *IEEE/ASME Trans. Mechatron.*, 2014, **19**, 312.
18 X. Liu, B. He, Z. Wang, H. Tang, T. Su and Q. Wang, *Sci. Rep.*, 2014, **4**, 6673, DOI: 10.1038/srep06673.
19 K. Jost, D. Stenger, C. R. Perez, J. K. McDonough, K. Lian, Y. Gogotsi and G. Dion, *Energy Environ.Sci.*, 2013, **6**, 2698.
20 X. Liu, D. Wu, H. Wang and Q. Wang, *Adv. Mater.*, 2014, **26**, 4370.
21 X. Liu, D. Wu, H. Wang, J. Yang and Q. Wang, *J. Mater. Chem. A*, 2014, **2**, 11569.
22 X. Liu, P. Shang, Y. Zhang, X. Wang, Z. Fan, B. Wang and Y. Zheng, *J. Mater. Chem. A*, 2014, **2**, 15273.
23 J.-H. Shin, W. A. Henderson and S. Passerini, *J. Electrochem. Soc.*, 2005, **152**, A978.
24 D. Qin, Y. Zhang, S. Huang, Y. Luo, D. Li and Q. Meng, *Electrochim. Acta*, 2011, **56**, 8680.
25 B. Lin, L. Qiu, J. Lu and F. Yan, *Chem. Mater.*, 2010, **22**, 6718.
26 J. Le Bideau, L. Viau and A. Vioux, *Chem. Soc. Rev.*, 2011, **40**, 907.
27 M. C. Gutiérrez, M. L. Ferrer and F. del Monte, *Chem. Mater.*, 2008, **20**, 634.
28 L. Qian and H. Zhang, *J. Chem. Technol. Biotechnol.*, 2011, **86**, 172.
29 J. Zhu, J. Wang, Q. Liu, Y. Liu, L. Wang, C. He and H. Wang, *J. Mater. Chem. B*, 2013, **1**, 978.
30 M. Barrow, A. Eltmimi, A. Ahmed, P. Myers and H. Zhang, *J. Mater. Chem.*, 2012, **22**, 11615.
31 H. Zhang, I. Hussain, M. Brust, M. F. Butler, S. P. Rannard and A. I. Cooper, *Nat. Mater.*, 2005, **4**, 787.
32 H. Bai, A. Polini, B. Delattre and A. P. Tomsia, *Chem. Mater.*, 2013, **25**, 4551.
33 C. V. Nicholas, D. J. Wilson, C. Booth and J. R. Giles, *Br. Polym. J.*, 1988, **20**, 289.
34 S. Dong, B. Zheng, D. Xu, X. Yan, M. Zhang and F. Huang, *Adv. Mater.*, 2012, **24**, 3191.
35 G. Yu, X. Yan, C. Han and F. Huang, *Chem. Soc. Rev.*, 2013, **42**, 6697.
36 D. Zhang, J. Yang, S. Bao, Q. Wu and Q. Wang, *Sci. Rep.*, 2013, **3**, 1399, DOI: 10.1038/srep01399.
37 K. Xie, X. Qin, X. Wang, Y. Wang, H. Tao, Q. Wu, L. Yang and Z. Hu, *Adv. Mater.*, 2012, **24**, 347.
38 W. Li, Z. Zhang, B. Han, S. Hu, Y. Xie and G. Yang, *J. Phys. Chem. B*, 2007, **111**, 6452.
39 A. R. Choudhury, N. Winterton, A. Steiner, A. I. Cooper and K. A. Johnson, *J. Am. Chem. Soc.*, 2005, **127**, 16792.

